ACS APPLIED MATERIALS & INTERFACES
Research Article
www.acsami.org

Three-Dimensional Printing of pH-Responsive and Functional Polymers on an Affordable Desktop Printer

Milena Nadgorny, Zeyun Xiao, Chao Chen, and Luke A. Connal*

Department of Chemical and Biomolecular Engineering, The University of Melbourne, Parkville, Victoria, 3010 Australia

S *Supporting Information*

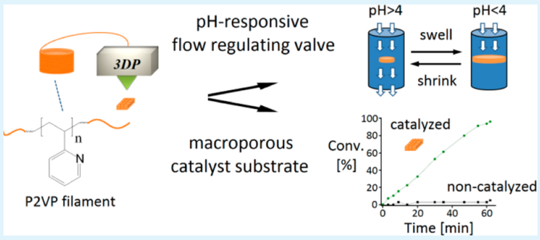

ABSTRACT: In this work we describe the synthesis, thermal and rheological characterization, hot-melt extrusion, and three-dimensional printing (3DP) of poly(2-vinylpyridine) (P2VP). We investigate the effect of thermal processing conditions on physical properties of produced filaments in order to achieve high quality, 3D-printable filaments for material extrusion 3DP (ME3DP). Mechanical properties and processing performances of P2VP were enhanced by addition of 12 wt % acrylonitrile−butadiene−styrene (ABS), which reinforced P2VP fibers. We 3D-print P2VP filaments using an affordable 3D printer. The pyridine moieties are cross-linked and quaternized postprinting to form 3D-printed pH-responsive hydrogels. The printed objects exhibited dynamic and reversible pH-dependent swelling. These hydrogels act as flow-regulating valves, controlling the flow rate with pH. Additionally, a macroporous P2VP membrane was 3D-printed and the coordinating ability of the pyridyl groups was employed to immobilize silver precursors on its surface. After the reduction of silver ions, the structure was used to catalyze the reduction of 4-nitrophenol to 4-aminophenol with a high efficiency. This is a facile technique to print recyclable catalytic objects.

KEYWORDS: *functional materials, 3D-printing, filaments, pH-responsive materials, catalysis, hot-melt extrusion*

■ INTRODUCTION

Three-dimensional printing (3DP) is rapidly gaining momentum as an enabling technology. This software-controlled, on-demand additive manufacturing technology provides personalized solutions to advanced fabrication needs with minimal waste and significantly streamlined costs and time.[1,2] Printed objects have enabled a broad range of applications, including tissue engineering,[3,4] pharmaceutics,[1,5] electronics,[1,6] robotics,[7] and anion exchange membranes.[8] Numerous additive manufacturing processes have been developed. However, most 3DP equipment is expensive and not always affordable.[1] Among the available 3DP processes, material extrusion 3DP (ME3DP), also known as fused deposition modeling (FDM), is gaining popularity due to its operational simplicity and low cost.[2] Today, ME3DP machines can be purchased for a low price, some as low as US$500. Low cost makes ME3DP machines accessible for small companies and even for private home users.[1,5] In ME3DP, a polymeric filament is mechanically forced through a heated nozzle, which liquefies the polymer to a semimolten state. The material is deposited on top of a build tray, layer by layer, until a desired structure is formed.[1,2] Production of filaments for ME3DP is an essential step which includes polymer processing by hot-melt extrusion, during which raw materials are melted and compressed to become filaments with defined shape and properties.[9] The diameter of 3D-printable filaments must fit the inlet diameter of the printing nozzle, and exhibit structural integrity, strength, and low surface roughness. These characteristics are important for avoiding interruptions to continuous printing and can impact physical properties of fabricated parts.[9,10] Therefore, production of filaments by hot-melt extrusion requires a strict definition of processing conditions.

Recently, there is an increasing interest in stimuli-responsive materials, which undergo dynamic structural transformations when subjected to an external stimulus, such as pH, temperature, or light.[11] These "smart" materials have enabled the concept of "4D" printing.[12] These dynamic changes make stimuli-responsive polymers prospective candidates for sensing,[13] soft robotics,[14] and fabrication of electronic devices.[15] Peterson et al. pioneered 3DP of force sensors by integrating units of mechano-responsive spiropyran to poly(ε-caprolactone) polymers.[13] Recently, 3D-printed electrical devices based on shape-memory polymers,[15] and gold nanorod-containing capsules for laser-triggered biomolecules release have been reported.[16] Hart et al. synthesized and 3D-printed polycaprolactone derived polymers and silica nanoparticle composites via ink-jet printing.[17] Wang et al. fabricated metallic structures by initiating polymerization of metal chelating polymer brushes on the surface of 3D-printed structures.[18] Xu et al. 3D-printed artificial bones based on polycaprolactone/hydroxyapatite, which successfully mimicked the biomechanics of natural bones.[19] Although the field of 3D-printable materials evolves, there are still a limited number of functional polymers that are

Received: June 18, 2016
Accepted: October 3, 2016
Published: October 3, 2016

© 2016 American Chemical Society

DOI: 10.1021/acsami.6b07388

"printable". Expanding this toolbox will enable even more applications.[20]

In this work, we employed poly(2-vinylpyridine) (P2VP) for production of filaments and 3DP of dynamic objects. This well-known pH-responsive polymer exhibits a globule-to-coil transition upon protonation below pH 4.0.[11] The pH-responsiveness of P2VP makes it an attractive platform for applications such as pH-responsive membranes[21] and photonic gels.[22] To the best of our knowledge, no works so far have presented pH-responsive polymers as thermally processable and compatible with ME3DP technology. Moreover, pyridine chemistry is not limited to pH-responsiveness but rather offers additional opportunities for functionalization, such as formation of coordination complexes with metals,[23] templating of mesostructured oxides,[24,25] and supramolecular self-assembly.[26,27]

Here, we first examine the thermal properties of P2VP and implement rheological tools for examination of its dynamic viscoelastic properties. We investigate the effect of thermal processing conditions on physical and morphological properties of P2VP filaments and determine an optimal temperature range for P2VP extrusion. Finally, we demonstrate 3DP capabilities with P2VP and show that its versatile postprinting functionalization can be successfully applicable as a platform for manufacturing of flow-regulating devices and catalytic supports.

■ EXPERIMENTAL SECTION

Materials. Tetrahydrofuran (THF, VWR Australia, 99.9%), diethyl ether (Chem-Supply, 99.5%) *N*,*N*-dimethylformamide (DMF, VWR Australia, 99.9%), 2-(dodecylthiocarbonothioylthio)-2-methylpropionic acid (DDMAT, Sigma-Aldrich, 98%), acrylonitrile−butadiene−styrene (ABS, Filabot, 448T grade), silver nitrate (Ajax Finechem), sodium borohydride (Scharlab, 98%), 1,4-dibromobutane (DBB, Sigma-Aldrich, 99%), 1-bromoethane (BE, Sigma-Aldrich, 99%), 4-nitrophenol (Sigma-Aldrich, 95%), ethanol (VWR Australia, 96%), acetone (Chem-Supply, 99.8%), *n*-hexane (RCI Labscan, 95%), hydrochloric acid (HCl, Ajax Finechem, 36%), nitric acid (Thermo Fisher, 70%), sodium hydroxide (VWR Australia, 99.6%), and lithium bromide (LiBr, >99%, Aldrich) were obtained. 2-Vinylpyridine (2VP, Sigma-Aldrich, 97%) was passed through a basic alumina column to remove the inhibitor, and 1,1′-azobis(cyclohexanecarbonitrile) (ACHN, Sigma-Aldrich, 98%) was recrystallized from ethanol and dried overnight prior to use. All other materials were used as received.

Instrumentation. Size exclusion chromatography (SEC) was performed on the Shimadzu liquid chromatography system with Phenomenex Phenogel columns, and DMF with 0.05 mol/L LiBr as an eluent at 70 °C with a flow rate of 1 mL/min. Average molecular weights (M_n, M_w) and polydispersity index (Đ) were calculated based on polystyrene calibration standards. Nuclear magnetic resonance (^{13}C NMR, ^{1}H NMR) was performed on a Varian 400 MHz spectrometer. Thermogravimetric analysis (TGA) was performed on a PerkinElmer Diamond instrument. The powder was placed in an alumina crucible and heated from 30 to 600 °C at a rate of 10 °C/min under an air flow of 1 mL/min. Dynamic mechanical analysis (DMA) was performed on a controlled stress rheometer with parallel plates geometry with a diameter of 40 mm (AR-G2, TA Instruments). Polymer extrusion for filament production was performed on a single screw extruder, rotating at a constant speed of 35 rpm (Filabot Original, Filabot) with a 1.60 mm diameter self-designed nozzle. The 3D-printed objects were created with a MakerBot Replicator 2X (Makerbot, 1.75 mm nozzle inlet diameter). Printing parameters were nozzle temperature 220 °C, platform temperature 90 °C, and travel speed 100 mm/s. Computer models for 3DP object design (.stl format) were downloaded from the Makerbot database, and their dimensions were modified by Makerbot software. Fourier transform infrared spectroscopy (FTIR, Varian 7000, ATR mode) was used for the chemical analysis of 3D-printed objects. Surface morphology of the filaments was characterized by a field emission scanning electron microscope (Philips XL30) operated at 2.0 kV. The elemental analysis of the functionalized object was conducted by an FEI Quanta FEG 200 scanning electron microscope with EDS analyzer (Oxford Instrument INCA X-ACT, silicon drift detector). UV−vis absorbance was detected with a Shimadzu UV-1800 spectrophotometer and UV Probe software package. Inductively coupled plasma optical emission spectroscopy (ICP-OES, 720ES, Varian) was used for the quantitative analysis of silver loss into catalyzed solutions.

P2VP Synthesis and Characterization. 2VP (30.0 g, 285 mmol), ACHN (21.0 mg, 8.60×10^{-2} mmol), and DDMAT (157 mg, 0.430 mmol) were combined with DMF (31.6 mL) in a 250 mL Schlenk tube equipped with a magnetic stir bar and subjected to three cycles of freeze−pump−thaw. After degassing the reaction mixture was sealed under nitrogen and the Schlenk tube was placed in an oil bath set at 75 °C for 22 h. The reaction was quenched by placing the Schlenk tube in an ice bath. The polymer was precipitated into cold diethyl ether, filtered and collected, dissolved in THF, and precipitated again. A light pink powder was collected and dried overnight.

The chemical structure of P2VP was characterized by ^{1}H NMR. Dimethyl sulfoxide-d_6 (DMSO-d_6) was used as a solvent. Conversion was calculated by comparing the integration of vinyl double bond signals (δ = 5.39, 5.41 ppm) with saturated hydrocarbons of P2VP backbone (δ = 1.68, 2.21 ppm) by crude ^{1}H NMR. The product was synthesized with 40% conversion, M_n = 47 kDa and Đ = 1.50. Additionally, ^{13}C NMR and FTIR were used for characterization of the synthesized structure.

Preparation of P2VP−ABS Blends. ABS pellets were grinded by a ring milling device (LabTechnics, Australia) at 720 rpm for 30 s until a fine powder was obtained. Afterward, P2VP (88 wt %) and ABS (12 wt %) were mixed for 10 s.

Rheology. The examined sample (0.70 g) was compressed into a 40 mm diameter slag. A compressed disk was placed between the parallel plates after zero gap calibration, heated to 200 °C, and ramped down to 80 °C.[28] The samples were examined under a frequency of 1 Hz at 0.3% strain, which is within the linear viscoelastic region, as was previously determined by the strain sweep experiment.

Extrusion. The polymers were added to the extruder at a constant rate, keeping the hopper full. The P2VP−ABS blend was extruded at the temperature range 145−195 °C. Filaments were collected for further analysis. The diameter of filaments was measured by an electronic caliper, and the density was calculated by dividing the weight of a filament fragment by its area.

Postprinting Quaternization and Cross-Linking. 3D-printed objects were cross-linked with DBB and quaternized with BE.[22] The reagents were added to an *n*-hexane (80 vol %) and acetone (20 vol %) mixture and stirred for 10 min. Immediately afterward, 3D-printed objects were placed in the reaction vessel, sealed, and placed in the oil bath at 40 °C for 15 h. The objects were then removed, rinsed with *n*-hexane, and allowed to dry overnight. A small piece was cut from the object and analyzed by FTIR.

For cross-linking only, molar ratios of DBB to P2VP repeating unit were 0.70 and 0.05 (samples 3D-$P2VP_{C70}$ and 3D-$P2VP_{C5}$, respectively). For quaternization and cross-linking molar ratios of DBB and BE to P2VP repeating unit were 0.05 and 0.20, respectively (sample 3D-$P2VP_{C5Q20}$).

Determination of Degree of Swelling. The degree of swelling was calculated according to eq 1:

$$\%S = [(W_w - W_d)/W_d] \times 100\% \qquad (1)$$

where W_d is the dry weight of the object, W_w is the weight of the object after submersion into the solution, and %*S* is the degree of swelling in percent.[29] To measure the degree of swelling, the object was taken from the solution, gently wiped to remove excess surface water, and weighed.

Flow Rate Measurement. A 3D-printed cross-linked and quaternized object was immobilized by a heat gun on the bottom of a glass tube (3D-$P2VP_{C5Q20}$, dimensions 0.3 cm × 0.3 cm × 0.3 cm, 80% infill). Constant volumes (15 mL) of solutions with different pH values (2.0, 2.5, 3.0, 3.5, 7.0, 10.0, and 13.0) were introduced to the

Scheme 1. Synthesis of P2VP by RAFT Polymerization

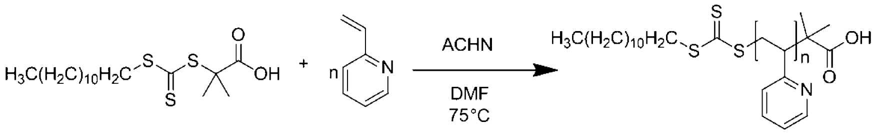

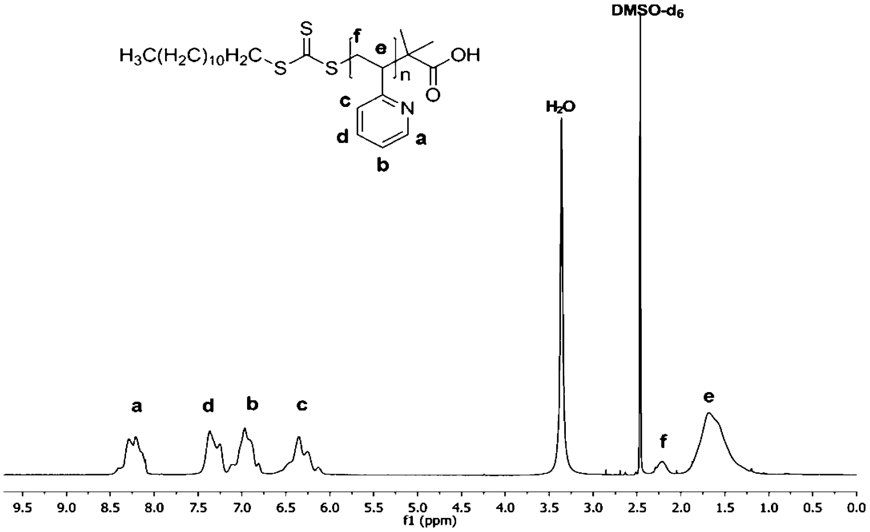

Figure 1. ^{1}H NMR spectrum of P2VP in DMSO-d_6. Formation of broad peaks in the aromatic region (a−d) and the appearance of peaks in the region of saturated hydrocarbons (e and f) support a successful synthesis of P2VP.

tube, and the time required for the liquid to flow through the tube was monitored with a stopwatch. First, sodium hydroxide solution (pH 13.0) was introduced to the tube, and then other solutions with decreasing pH values (from 13.0 to 2.0) were injected one by one. Three continuous cycles of this experiment were conducted.

Preparation of 3D-Printed Catalytic Membrane. A 3D-printed object (0.174 g, 0.9 cm × 0.9 cm × 0.5 cm, 50% infill) was submerged into 20 mM aqueous $AgNO_3$ solution (0.117 g of $AgNO_3$, 34.5 mL of deionized water) overnight. The sample was then introduced to $NaBH_4$ solution (0.076 g of $NaBH_4$, 30.5 mL of deionized water) by direct pipetting and dried under nitrogen.[23]

Catalyzed Reduction of 4-Nitrophenol.[30] 4-Nitrophenol solution (240 μL, 0.002 M) was mixed with aqueous $NaBH_4$ solution (16.0 mL, 0.06 M) and deionized water (13.4 mL) and introduced to the catalytic membrane. To follow the catalytic activity, a fraction was collected from the reaction vessel at specified time intervals and examined under UV−vis. Three cycles of catalytic reaction were performed continuously.

Analysis of Silver Leaching. Detection of silver traces in collected fractions of 4-aminophenol solutions was conducted by ICP-OES analysis. After each catalytic cycle, 2 mL of the finally collected fraction was diluted by addition of 2 mL of nitric acid (5% in water) and filtered. Silver concentrations were calculated from calibration curves based on silver standards.

■ RESULTS AND DISCUSSION

Reversible addition−fragmentation chain transfer (RAFT) polymerization was utilized to prepare well-defined P2VP (M_n = 47 kDa, Đ = 1.50). See Scheme 1 for the synthesis, Figure S1 for the SEC chromatogram, Figure S2 for crude ^{1}H NMR, Figure S3 for ^{13}C NMR, and Figure S4 for FTIR spectra. Structural confirmation was also performed by ^{1}H NMR. The spectrum shows the formation of broad signals at δ = 8.25, 7.35, 6.96, and 6.35 ppm, which correspond to P2VP aromatic protons. Signals at δ = 2.21 and δ = 1.68 ppm are attributed to saturated hydrocarbons forming the P2VP backbone (Figure 1).

To be ME3DP compatible, polymers must obtain a balanced flexibility and rigidity to retain their structural integrity. Successful materials must not deform or break while filaments are loaded or being printed. Our initial attempts to extrude P2VP at a broad range of temperatures (140−190 °C) without external additives yielded fragile filaments which defragmented when they were pushed through the nozzle. We therefore tried to improve the mechanical properties of P2VP filaments by adding a small fraction of ABS (12 wt %). ABS is the most used thermoplastic material in ME3DP;[2] it is known for its toughening properties and outstanding mechanical characteristics.[31] As a result of ABS addition, the mechanical properties of P2VP filaments significantly improved. The produced filaments could successfully withstand the entire processing workflow without any signs of damage. The storage modulus of P2VP−ABS blend increased when compared with that of neat P2VP, which demonstrates the reinforcement effect of ABS (Figure S5).

Viscoelastic properties of polymers play a key role in the assessment of their processing conditions.[28] To determine the glass transition temperature (T_g), at which polymer chains have enough thermal energy for a free motion, begin to disentangle and flow, DMA was performed[28] (oscillatory strain sweep is shown in Figure S6). The T_g of P2VP−ABS blend is 120 °C, which is represented by the maximum of the tan delta curve (Figure 2). A single peak demonstrates that ABS is miscible in P2VP.[32] While the T_g of neat P2VP is 124 °C (Figure S7), the addition of ABS shifts the peak of tan delta toward 120 °C due to the presence of ABS. The T_g of styrene−acrylonitrile (SAN) polymer in ABS is 116 °C, as was previously reported in the literature.[31,33] Therefore, the peak of the blend is located in the region between 116 and 124 °C. The viscosity of P2VP−ABS

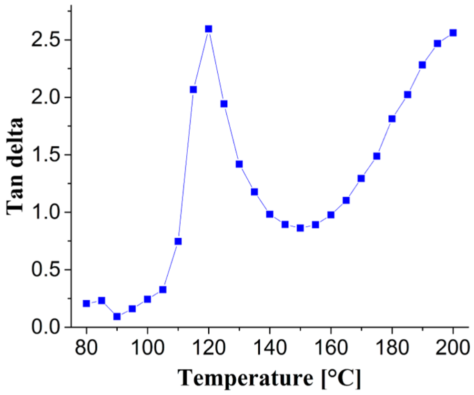

Figure 2. Loss tangent of P2VP−ABS blend exhibits a single maximum at 120 °C indicating the T_g.

blend exhibits shear thinning, which makes the blend suitable for extrusion processing. At the high shear region the viscosity reaches 0.4 Pa·s (Figure S8).

The TGA profile of P2VP−ABS blend shows that the degradation temperature is 360 °C, above which approximately 60% of the initial weight is lost (Figure 3). A small weight loss observed at 108 °C is attributed to the evaporation of the absorbed moisture. TGA results, therefore, indicate that the blend is stable and can be processed below 360 °C. These findings are also supported by SEC analysis before and after thermal processing, which indicates the chemical stability of the polymer (Figure S9).

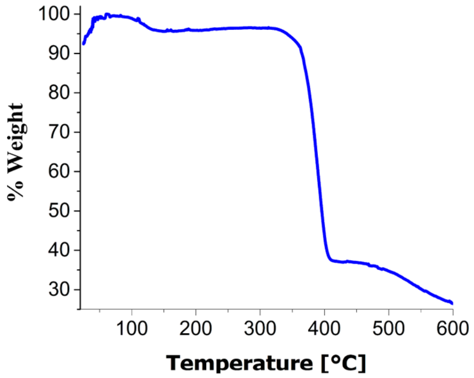

Figure 3. TGA plot of P2VP−ABS blend indicates that the blend is thermally stable below 360 °C.

To comply with ME3DP, the diameter of produced filaments must be strictly defined. During extrusion, polymers are subjected to high shear and compression forces. When melts are subjected to shear, they develop normal stresses, which are unevenly distributed in the direction of the flow and perpendicular to the flow direction due to the polymers' anisotropic microstructure.[34] After exiting the die, the extrudate swells to recover from caused deformations, the phenomenon which is known as die swell.[9,34,35] Die swell is highly undesirable during filament production since the diameter of the filament must not exceed the inlet diameter of the printing nozzle (1.75 mm with 0.05 mm tolerance). Several strategies to minimize the die swell effect are known, such as optimization of extruder geometry and control of rotation speed, temperature, and flow rate.[34,35] Since the geometry and the rotation speed of our extrusion system are not variable, we controlled the die swell by adjusting the flow rate and the temperature of the blend. A self-designed nozzle with a diameter of 1.60 mm was used to compensate for the die swell effect. When the diameter of the nozzle decreases, the residence time of the polymer inside the extruder increases, which allows more time for relaxation processes and therefore decreases the swelling.[9,34,35] When a standard 1.75 mm nozzle was used in preliminary studies, the diameter of produced filaments exceeded 1.80 mm for a wide range of extrusion temperatures, which made the filaments unsuitable for 3DP.

To optimize the process of filament production by hot-melt extrusion, we investigated the effect of extrusion temperature on the filaments' physical properties. The diameter and density of filaments as a function of extrusion temperatures are summarized in Table 1. When the extrusion temperature was set between 145 and 165 °C, the diameter of the filaments constantly remained 1.70 mm. At 175 °C the diameter increased to 1.80 mm. These diameters are within the optimal range to meet ME3DP requirements. When the extrusion temperature exceeded 175 °C, the diameter of the filaments drastically increased and reached 2.0 and 2.05 mm at 185 and 195 °C, respectively, making these filaments unsuitable for 3DP (Figure 4a).

Table 1. Summary of Physical Characteristics of the Extruded Filaments (Average of Two Measurements ± Standard Deviation)

extrusion temp [°C]	diameter [mm]	density [g/cm^3]
145	1.70 ± 0.00	1.29 ± 0.02
155	1.70 ± 0.00	1.26 ± 0.02
165	1.70 ± 0.07	1.26 ± 0.04
175	1.80 ± 0.07	1.25 ± 0.05
185	2.00 ± 0.07	1.11 ± 0.07
195	2.05 ± 0.21	1.08 ± 0.18

The density of filaments is another important characteristic for printing quality. When extrusion temperatures are exceedingly high, air bubbles are trapped in the melt. As a result, a filament develops internal voids, which may result in discontinuous printing and deterioration in a structural integrity of a printed part.[10] A study of filament density shows that, below 175 °C, the density is not significantly affected by temperature variations. At 145 °C the density of the filament is 1.29 g/cm^3, the highest in the examined temperature range. With further increase in temperature, the density slightly decreases and remains constant in the range of 1.25−1.26 g/cm^3, as can be concluded from the plateau of the curve in Figure 4b. Above 175 °C, the density sharply drops to 1.11 and 1.08 g/cm^3 when the extrusion temperature is 185 and 195 °C, respectively.

A simultaneous increase in filament diameter and a sharp decrease in density above 175 °C suggest that air bubbles are trapped inside the filament. SEM characterization demonstrates a gradual increase in surface roughness with the increase in extrusion temperature (Figure 5). At 165 °C, the filament is smooth and does not exhibit noticed surface defects (Figure 5a). At 175 °C, the surface roughness slightly increases (Figure 5b). Above 185 °C, the surface becomes exceedingly rough with multiple defects and local microfractures (Figure 5c,d). The increase in the surface roughness with the increase in extrusion temperature is attributed to internal deformations of the filament caused by the trapped air.

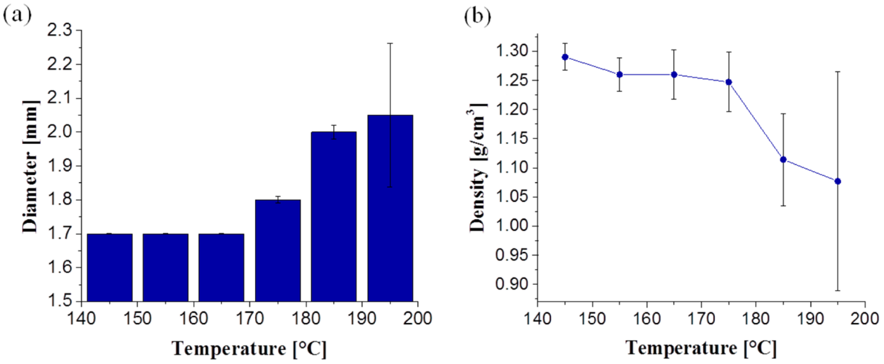

Figure 4. Effect of extrusion temperature on characteristics of produced filaments: (a) filament diameter; (b) filament density. Above 175 °C, the diameter of filaments drastically increases and the density decreases.

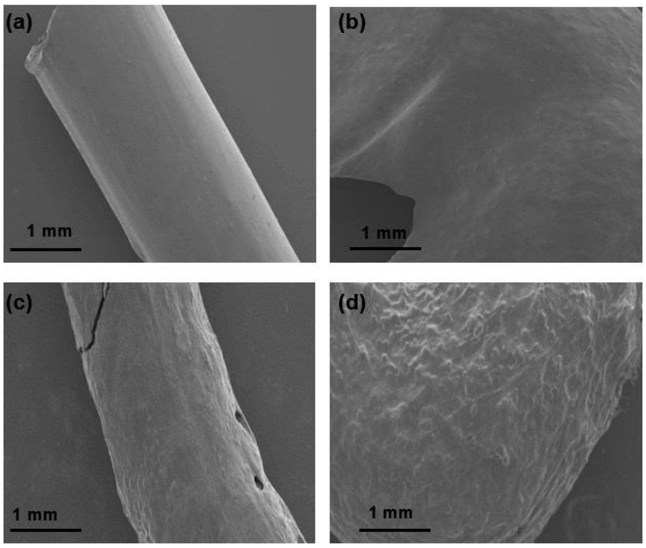

Figure 5. SEM images of P2VP filaments produced at different extrusion temperatures: (a) 165, (b) 175, (c) 185, and (d) 195 °C. Surface roughness gradually increases with the increase in extrusion temperature.

Based on the characteristics shown above, the range of optimal extrusion temperatures which yield filaments with sufficiently high density, 1.70−1.80 mm diameter, and a smooth surface is 145−175 °C. Below 140 °C, the extrusion was found ineffective due to an extremely slow and noncontinuous mass flow. The produced filaments (Figure 6a) were successfully used for 3DP of objects such as starfish or a seahorse (Figure 6b), which were 3D-printed within approximately 15 min and exhibited a high printing quality.

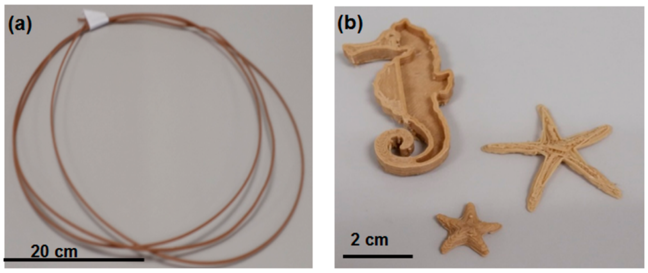

Figure 6. (a) Filaments produced by hot-melt extrusion. (b) 3D-printed P2VP objects: starfish and a seahorse.

Rectangular slabs (8.0 mm × 16.0 mm × 2.0 mm, 80% infill) were 3D-printed for the preparation of pH-responsive hydrogels. The 3D-printed objects were cross-linked with DBB to give the objects structural integrity and quaternized with BE to enable further swelling properties to the 3D-printed hydrogels. The FTIR spectrum reveals the formation of peaks at 1589 and 1568 cm^{-1}, which represent C═C stretching vibration of pyridine rings. Formation of a band at 1639 cm^{-1} indicates that the quaternization was successful due to formation of the characteristic pyridinium band[29,36] (Figure 7a). The intensity of the pyridinium band increases with the increasing fraction of quaternizing reagents, while no peak is seen in the unmodified object (3D-P2VP). After the reactions, printed slabs become pale brown with white coloration, possibly due to the conversion of pyridine to pyridinium salt. Quaternized and cross-linked objects were dipped into aqueous HCl solutions (pH 2.0) to investigate swelling properties. The swelling dynamics of printed objects was studied by tracking the change in the objects' degree of swelling at defined time intervals. Dynamic swelling curves indicate a rapid water uptake by quaternized and cross-linked P2VP (Figure 7b). Control of the polymer structure, for example the cross-linking density (by DBB stoichiometry) and the final charge (by BE addition), gave access to dramatically different swelling profiles. Swelling characteristics are summarized in Table 2. The 3D-printed object cross-linked with DBB (3D-P2VP$_{C5}$) exhibits a rapid increase in weight. The degree of swelling reaches 69% after 40 s of exposure to HCl solution. After 24 h, the degree of swelling reaches an equilibrium value of 97%. When the molar ratio of DBB to P2VP repeating unit increased to 0.70 (3D-P2VP$_{C70}$), the degree of swelling became significantly lower. During the first 10 s the object swelled by 43%. The uptake of water plateaued and reached an equilibrium of only 57% after 24 h. In order to gain further responsive behavior, the remaining pyridine groups of the cross-linked 3D-printed object were quaternized with BE to increase the charge of P2VP. This cross-linked and hydrophilic gel (3D-P2VP$_{C5Q20}$) shows a different swelling profile with a significant water uptake within the first 10 s of exposure to the acidic solution, reaching 107% swelling. After 22 h, the swollen object reached its equilibrium swelling of 125%. The swelling of both cross-linked and cross-linked and quaternized objects is attributed to the formation of a positive charge on pyridine groups. While cross-linking with DBB charges P2VP, it also forms a physical barrier by cross-linking P2VP, which constrains the swelling. Therefore, the degree of swelling decreases with the increasing concentration of DBB. Additional quaternization with BE increases the charge on

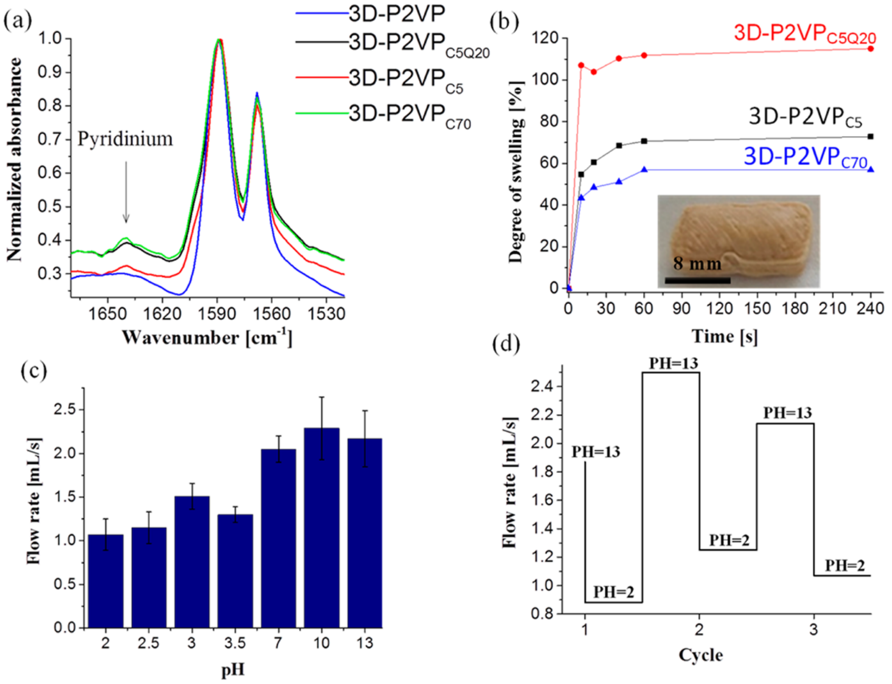

Figure 7. Quaternization and cross-linking of 3D-printed P2VP objects and demonstration of their pH-responsiveness. (a) FTIR spectra of 3D-printed objects: unreacted P2VP object (3D-P2VP), object cross-linked with different ratios of DBB (3D-P2VP$_{C70}$ and 3D-P2VP$_{C5}$), and object cross-linked with DBB and quaternized with BE (3D-P2VP$_{C5Q20}$). Reacted objects show a formation of pyridinium peak at 1639 cm^{-1} (marked by an arrow). (b) Dynamic swelling of 3D-printed objects shows control over swelling properties by controlling the pyridine chemistry; with increased cross-linking density (3D-P2VP$_{C70}$) minimal swelling is observed, with decreased cross-linking density (3D-P2VP$_{C5}$) increased swelling is observed, and with minimal cross-linking and further quaternization of the pyridyl groups (3D-P2VP$_{C5Q20}$) a substantial increase in swelling is observed. The inset shows a quaternized and cross-linked 3D-printed object (3D-P2VP$_{C5Q20}$) in its swollen state. (c) Cross-linked and quaternized 3D-printed P2VP application as a flow-regulating valve: flow rate as a function of pH (average of three measurements ± standard deviation). (d) pH-dependent, reversible flow control is achieved by swelling and shrinking of 3D-printed P2VP.

Table 2. Summary of Swelling Characteristics of 3D-Printed, Cross-Linked, and Quaternized P2VP Objects[a]

sample	molar ratio of P2VP repeating unit/DBB/BE	equilib swelling [%]
3D-P2VP$_{C70}$	1/0.70/0	57
3D-P2VP$_{C5}$	1/0.05/0	97
3D-P2VP$_{C5Q20}$	1/0.05/0.20	125

[a] The degree of swelling decreases with a higher degree of cross-linking and increases with quaternization by BE.

pyridine rings, which enhances interactions with water. Therefore, when BE is added the rate of water uptake increases and also reaches higher equilibrium values than objects which were not introduced to BE.

When the object was not treated with BE and DBB (3D-P2VP), almost full solubilization occurred within 24 h of submersion into HCl. Only small traces of the printed object were left, which mostly contained residual ABS.

Dynamic swelling of P2VP was used as a principle for fabrication of a flow regulating device.

The experimental setup of the system is presented in Figure S10. A P2VP object was 3D-printed to fit into a glass capillary; upon cross-linking and quaternization we investigated the pH-dependent regulation of water flow through the capillary (Figure 7c). When pH values were 7.0, 10.0, and 13.0, average flow rates were 2.05, 2.29, and 2.17 mL/s, respectively. When the pH decreased to 3.5, flow rates decreased by approximately 30%. Below pH 3.0, flow rates further decreased to 1.51, 1.15, and 1.07 mL/s at pH 3.0, 2.5 and 2.0, respectively. This sharp decrease in flow rates is attributed to P2VP protonation below pH 4.0, which induces P2VP transformation from globule to coil state.[11] As a result, flow restrictions are caused by a physical blocking of the tube outlet by swollen P2VP. The reversibility of the process was also investigated. When a P2VP valve is introduced to an acidic solution (pH 2.0), P2VP swells and therefore the flow rate decreases. When an alkaline solution (pH 13.0) is injected into the tube, P2VP deprotonates and shrinks, which causes the recovery of the flow (Figure 7d). These dynamic properties make 3D-printed P2VP successfully applicable as a pH-responsive, flow-regulating valve.

To demonstrate P2VP chemical versatility and to explore its broad applicability beyond pH-responsiveness, the ability of our 3D-printed system to interact with metals was studied. Metal nanoparticles are of great interest due to their unique optical, electrical, and catalytic properties.[23,30] Silver nanoparticles are known as efficient catalysts for organic reactions, such as oxidation of styrene[37] and reduction of aromatic nitro-compounds.[30] These catalytic reactions are usually conducted by dispersing a metal catalyst in a solution. To prevent the agglomeration of nanoparticles, surfactants are used as stabilizers which interact with the surface of nanoparticles. Since the catalysis is mainly a surface reaction, the catalytic activity is prone to inhibition.[30] Other approaches include utilization of polymeric supports with loaded catalysts.[30,38] The efficiency of these methods is still limited since they require purification steps to separate, remove, and recycle the catalyst after the reaction is accomplished.

Pyridines are known for their ability to form coordination complexes with transition metals via nitrogen atoms.[23,25] By

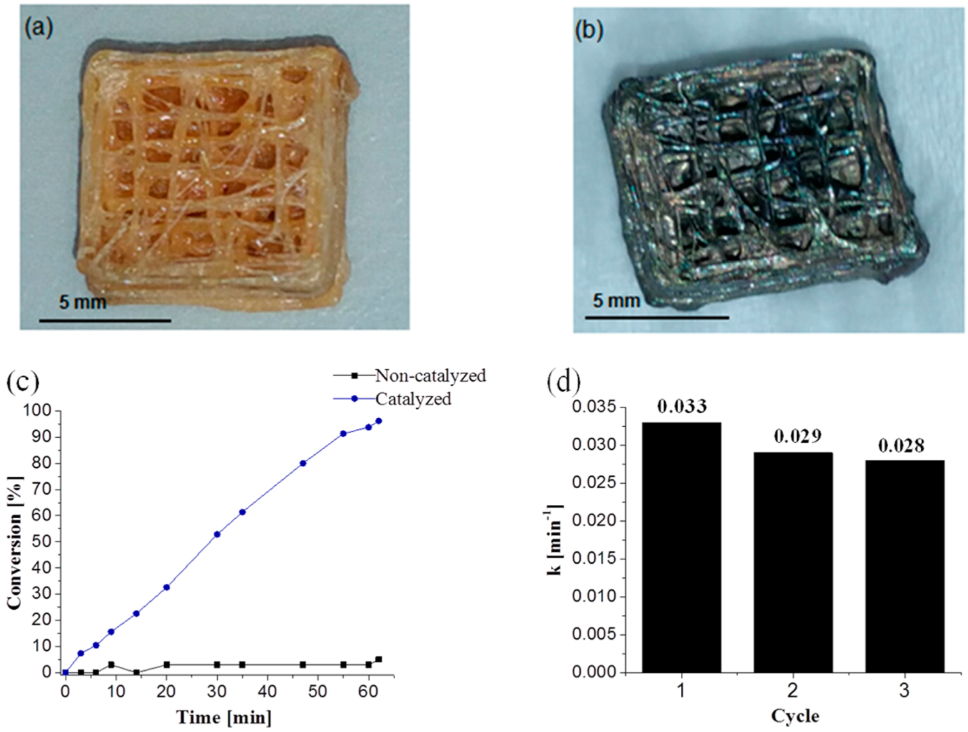

Figure 8. Preparation and evaluation of 3D-printed Ag-functionalized catalytic objects. (a) 3D-printed macroporous P2VP structure before functionalization. (b) P2VP structure after reaction with silver precursor and reduction. (c) Catalytic activity of Ag-functionalized, 3D-printed P2VP; the reaction of 4-nitrophenol reduction reaches almost full conversion after 62 min. (d) Reaction constants of 4-nitrophenol reduction in the presence of Ag-functionalized P2VP remain stable within three continuous cycles.

utilizing 3DP capabilities to design objects with advanced architectures, we fabricated a macroporous P2VP membrane which acts as a heterogeneous catalyst support in a single-step reduction of 4-nitrophenol to 4-aminophenol. This novel approach eliminates the need for costly and time-consuming separation processes. P2VP filaments were used for 3D-printing of a macroporous structure (Figure 8a). The object was reacted with silver nitrate and then reduced. After the reduction, dark coloration was observed due to formation of a silver layer on the surface of the object (Figure 8b). Energy-dispersive X-ray spectroscopy indicates that the surface is densely covered with silver (77.72 wt %, 29.45 atom %; Figure S11).

To demonstrate the catalytic activity of 3D-printed Ag-functionalized P2VP, we investigated the catalysis of 4-nitrophenol reduction. 4-Nitrophenol is recognized as an environmentally hazardous material. Since the compound is not degradable, 4-nitrophenol treatment is of a high importance for environmental considerations.[38] We placed the 3D-printed Ag-functionalized P2VP into a glass column, added aqueous 4-nitrophenol solution, and monitored the catalysis at room temperature. To follow the catalytic activity, we collected a fraction from the column at specified time intervals, and applied UV−vis to monitor the conversion of 4-nitrophenol to 4-aminophenol. The absorbance at 400 nm, attributed to 4-nitrophenolate ion, gradually decreased with the reaction time, while a 310 nm aminophenol peak appeared (Figure S12a).[30,38] These changes can be also visually monitored by a gradual decay in a yellow color with the reaction time. Around 96% conversion is reached after 62 min, while without the catalyst the reaction does not take place even after 24 h (Figure 8c). The calculated apparent rate constant of this pseudo-first-order reaction is 0.033 min^{-1} (Figure S12b). The apparent rate constant is lower than previously reported in the literature[30,38] potentially due to significantly larger reaction scales. The 3D-printed Ag-functionalized P2VP retained its catalytic activity for three continuous reaction cycles without showing any significant decrease in the reaction rate (Figure 8d). Moreover, silver leaching from the 3D-printed object into the solution was assessed after the completion of each catalytic cycle. ICP-OES analysis indicates the presence of very low silver amounts in the catalyzed solutions, which increases with the number of catalytic cycles. After the first, second, and third catalytic cycles, respectively, 0.42, 0.54, and 0.64 ppm silver were found in the solution. These low concentrations of silver represent 0.035 (cycle 1), 0.045 (cycle 2), and 0.052% (cycle 3) loss of the initial silver load on the surface of the 3D-printed structure. These results indicate that only a negligible loss of silver occurs during the reaction and therefore the catalytic structure is stable. After the reaction, the 3D-printed catalytic membrane was easily removed from the column, without additional separation steps for the catalyst recycling.

■ CONCLUSIONS

In this work, we present for the first time P2VP as thermally processable and 3D-printable material with versatile applications. We demonstrated that an easily synthesized pH-responsive polymer can be extruded and 3D-printed using affordable and easily accessible technologies. Addition of ABS to P2VP as a reinforcing material efficiently enhanced the mechanical stability of P2VP, which was initially prone to damages caused by the 3DP process. First, we show that processing conditions, such as temperature, play a critical role in the filament production process. Then, we demonstrate the printing capabilities of both simple and advanced macroporous structures. We perform a postprinting functionalization of

P2VP by quaternizing and cross-linking 3D-printed P2VP objects. The postprinting functionalization approach was extremely effective, as shown by FTIR study and dynamic swelling experiments. We demonstrated that the degree of swelling can be precisely tuned by a choice of quaternizing reagents and their stoichiometry. More importantly, postprinting functionalization strategy addresses current limitations of ME3DP materials,[1] allowing 3D-printing of polymers which are functionalized to become hydrogels in a single-step reaction. Therefore, the postprinting functionalization approach expands the applicability of ME3DP for an even broader scope of applications. We also demonstrated that 3D-printed P2VP can coordinate with metal precursors, which can be utilized as 3D-printed catalytic objects. Heterogeneous catalysis mediated by 3D-printed P2VP eliminates the usage of harmful chemicals and streamlines operational time and costs needed for catalyst separation and recycling without compromising on reaction efficiency.

■ ASSOCIATED CONTENT

Ⓢ Supporting Information

The Supporting Information is available free of charge on the ACS Publications website at DOI: 10.1021/acsami.6b07388.

> SEC traces, crude ^{1}H NMR, ^{13}C NMR, and FTIR spectrograms, rheological characterization, captions of the flow-regulating setup, EDS analysis, and catalysis kinetics study by UV−vis (PDF)

■ AUTHOR INFORMATION

Corresponding Author

*E-mail: luke.connal@unimelb.edu.au.

Author Contributions

The manuscript was written through contributions of all authors. All authors have given approval to the final version of the manuscript.

Funding

This work was supported by the Victorian Endowment for Science Knowledge and Innovation (L.A.C.).

Notes

The authors declare no competing financial interest.

■ ACKNOWLEDGMENTS

The authors would like to thank Bio21 Advanced Microscopy Facility for technical assistance with EDS analysis and Armeneh Hassanvand for assistance with ICP-OES analysis.

■ ABBREVIATIONS

P2VP, poly(2-vinylpyridine)
DBB, 1,4-dibromobutane
BE, 1-bromoethane
ACHN, 1,1′-azobis(cyclohexanecarbonitrile)
3DP, three-dimensional printing
ABS, acrylonitrile−butadiene−styrene
DDMAT, 2-(dodecylthiocarbonothioylthio)-2-methylpropionic acid
DMA, dynamic mechanical analysis
DMF, *N*,*N*-dimethylformamide
DMSO, dimethyl sulfoxide
FDM, fused deposition modeling
ME3DP, material extrusion 3D-printing
FTIR, Fourier transform infrared
RAFT, reversible addition−fragmentation chain transfer
SEC, size exclusion chromatography
NMR, nuclear magnetic resonance
THF, tetrahydrofuran
TGA, thermogravimetric analysis
2VP, 2-(vinylpyridine)
ICP-OES, inductively coupled plasma optical emission spectroscopy
SEM, scanning electron microscopy
EDS, energy dispersive X-ray spectroscopy
T_g, glass transition temperature

■ REFERENCES

(1) Gross, B. C.; Erkal, J. L.; Lockwood, S. Y.; Chen, C.; Spence, D. M. Evaluation of 3D Printing and Its Potential Impact on Biotechnology and the Chemical Sciences. *Anal. Chem.* **2014**, *86*, 3240−3253.

(2) Hofmann, M. 3D Printing Gets a Boost and Opportunities with Polymer Materials. *ACS Macro Lett.* **2014**, *3*, 382−386.

(3) Zein, I.; Hutmacher, D. W.; Tan, K. C.; Teoh, S. H. Fused Deposition Modeling of Novel Scaffold Architectures for Tissue Engineering Applications. *Biomaterials* **2002**, *23*, 1169−1185.

(4) Chia, H. N.; Wu, B. M. High-Resolution Direct 3D Printed PLGA Scaffolds: Print and Shrink. *Biofabrication* **2015**, *7*, 015002.

(5) Goyanes, A.; Wang, J.; Buanz, A.; Martínez-Pacheco, R.; Telford, R.; Gaisford, S.; Basit, A. W. 3D Printing of Medicines: Engineering Novel Oral Devices with Unique Design and Drug Release Characteristics. *Mol. Pharmaceutics* **2015**, *12*, 4077−4084.

(6) Kong, Y. L.; Tamargo, I. A.; Kim, H.; Johnson, B. N.; Gupta, M. K.; Koh, T.-W.; Chin, H.-A.; Steingart, D. A.; Rand, B. P.; McAlpine, M. C. 3D Printed Quantum Dot Light-Emitting Diodes. *Nano Lett.* **2014**, *14*, 7017−7023.

(7) Ilievski, F.; Mazzeo, A. D.; Shepherd, R. F.; Chen, X.; Whitesides, G. M. Soft Robotics for Chemists. *Angew. Chem.* **2011**, *123*, 1930−1935.

(8) Seo, J.; Kushner, D. I.; Hickner, M. A. 3D Printing of Micropatterned Anion Exchange Membranes. *ACS Appl. Mater. Interfaces* **2016**, *8*, 16656−16663.

(9) Nikzad, M.; Masood, S. H.; Sbarski, I. Thermo-Mechanical Properties of a Highly Filled Polymeric Composites for Fused Deposition Modeling. *Mater. Eng.* **2011**, *32*, 3448−3456.

(10) Yang, Y.; Chen, Y.; Wei, Y.; Li, Y. 3D Printing of Shape Memory Polymer for Functional Part Fabrication. *Int. J. Adv. Manuf. Technol.* **2016**, *84*, 2079.

(11) Liu, F.; Urban, M. W. Recent Advances and Challenges in Designing Stimuli-Responsive Polymers. *Prog. Polym. Sci.* **2010**, *35*, 3−23.

(12) Khoo, Z. X.; Teoh, J. E. M.; Liu, Y.; Chua, C. K.; Yang, S.; An, J.; Leong, K. F.; Yeong, W. Y. 3D Printing of Smart Materials: A Review on Recent Progresses in 4D Printing. *Virtual Phys. Prototyp.* **2015**, *10*, 103−122.

(13) Peterson, G. I.; Larsen, M. B.; Ganter, M. A.; Storti, D. W.; Boydston, A. J. 3D-Printed Mechanochromic Materials. *ACS Appl. Mater. Interfaces* **2015**, *7*, 577−583.

(14) Gossweiler, G. R.; Brown, C. L.; Hewage, G. B.; Sapiro-Gheiler, E.; Trautman, W. J.; Welshofer, G. W.; Craig, S. L. Mechanochemically Active Soft Robots. *ACS Appl. Mater. Interfaces* **2015**, *7*, 22431−22435.

(15) Zarek, M.; Layani, M.; Cooperstein, I.; Sachyani, E.; Cohn, D.; Magdassi, S. 3D Printing of Shape Memory Polymers for Flexible Electronic Devices. *Adv. Mater.* **2016**, *28*, 4449.

(16) Gupta, M. K.; Meng, F.; Johnson, B. N.; Kong, Y. L.; Tian, L.; Yeh, Y.-W.; Masters, N.; Singamaneni, S.; McAlpine, M. C. 3D Printed Programmable Release Capsules. *Nano Lett.* **2015**, *15*, 5321−5329.

(17) Hart, L. R.; Li, S.; Sturgess, C.; Wildman, R.; Jones, J. R.; Hayes, W. 3D Printing of Biocompatible Supramolecular Polymers and Their Composites. *ACS Appl. Mater. Interfaces* **2016**, *8*, 3115−3122.

(18) Wang, X.; Guo, Q.; Cai, X.; Zhou, S.; Kobe, B.; Yang, J. Initiator-Integrated 3D Printing Enables the Formation of Complex

Metallic Architectures. *ACS Appl. Mater. Interfaces* **2014**, *6*, 2583−2587.
(19) Xu, N.; Ye, X.; Wei, D.; Zhong, J.; Chen, Y.; Xu, G.; He, D. 3D Artificial Bones for Bone Repair Prepared by Computed Tomography-Guided Fused Deposition Modeling for Bone Repair. *ACS Appl. Mater. Interfaces* **2014**, *6*, 14952−14963.
(20) Oropallo, W.; Piegl, L. A. Ten Challenges in 3D Printing. *Eng. Comput.* **2016**, *32*, 135−148.
(21) Orlov, M.; Tokarev, I.; Scholl, A.; Doran, A.; Minko, S. pH-Responsive Thin Film Membranes from Poly (2-Vinylpyridine): Water Vapor-Induced Formation of a Microporous. *Macromolecules* **2007**, *40*, 2086−2091.
(22) Kang, Y.; Walish, J. J.; Gorishnyy, T.; Thomas, E. L. Broad-Wavelength-Range Chemically Tunable Block-Copolymer Photonic Gels. *Nat. Mater.* **2007**, *6*, 957−960.
(23) Dong, H.; Fey, E.; Gandelman, A.; Jones, W. E. Synthesis and Assembly of Metal Nanoparticles on Electrospun Poly (4-Vinylpyridine) Fibers and Poly (4-Vinylpyridine) Composite Fibers. *Chem. Mater.* **2006**, *18*, 2008−2011.
(24) Hayward, R. C.; Chmelka, B. F.; Kramer, E. J. Crosslinked Poly (Styrene)-block-poly (2-vinylpyridine) Thin Films as Swellable Templates for Mesostructured Silica and Titania. *Adv. Mater.* **2005**, *17*, 2591−2595.
(25) Connal, L. A.; Lynd, N. A.; Robb, M. J.; See, K. A.; Jang, S. G.; Spruell, J. M.; Hawker, C. J. Mesostructured Block Copolymer Nanoparticles: Versatile Templates for Hybrid Inorganic/organic Nanostructures. *Chem. Mater.* **2012**, *24*, 4036−4042.
(26) Chen, C.; Xiao, Z.; Connal, L. A. Phase Separated Block Copolymer Particles with Tuneable Morphologies: Striped, Onion, and Patchy Particles. *Aust. J. Chem.* **2016**, *69*, 741−745.
(27) Klinger, D.; Robb, M. J.; Spruell, J. M.; Lynd, N. A.; Hawker, C. J.; Connal, L. A. Supramolecular Guests in Solvent Driven Block Copolymer Assembly: From Internally Structured Nanoparticles to Micelles. *Polym. Chem.* **2013**, *4*, 5038−5042.
(28) Gupta, S. S.; Meena, A.; Parikh, T.; Serajuddin, A. T. Investigation of Thermal and Viscoelastic Properties of Polymers Relevant to Hot Melt Extrusion, I: Polyvinylpyrrolidone and Related Polymers. *J. Excipients Food Chem.* **2014**, *5*, 32−45.
(29) Huang, A.; Xiao, C.; Zhuang, L. Synthesis and Characterization of Quaternized Poly (4-vinylpyridine-co-styrene) Membranes. *J. Appl. Polym. Sci.* **2005**, *96*, 2146−2153.
(30) Shi, L.; Liu, M.; Liu, L.; Gao, W.; Su, M.; Ge, Y.; Zhang, H.; Dong, B. Magnetically Recyclable Polymer Single Crystal Supported Silver Nanocatalyst. *Langmuir* **2014**, *30*, 13456−13461.
(31) Li, Y.; Shimizu, H. Improvement in Toughness of Poly (L-lactide) (PLLA) through Reactive Blending with Acrylonitrile−butadiene−styrene Copolymer (ABS): Morphology and Properties. *Eur. Polym. J.* **2009**, *45*, 738−746.
(32) Komalan, C.; George, K. E.; Kumar, P. A. S.; Varughese, K. T.; Thomas, S. Dynamic Mechanical Analysis of Binary and Ternary Polymer Blends Based on Nylon copolymer/EPDM Rubber and EPM Grafted Maleic Anhydride Compatibilizer. *eXPRESS Polym. Lett.* **2007**, *1*, 641−653.
(33) Zitzumbo, R.; Avalos, F.; Alonso, S. Nanostructural Complex in ABS/TPU Immiscible Mixtures. *Polym. Polym. Compos.* **2016**, *24*, 205−212.
(34) Vlachopoulos, J.; Strutt, D. The Role of Rheology in Polymer Extrusion. Presented at the New Technology for Extrusion Conference, Milan, Italy, Nov 20−21, 2003.
(35) Liang, J. Z. Effects of Extrusion Conditions on Die-Swell Behavior of Polypropylene/diatomite Composite Melts. *Polym. Test.* **2008**, *27*, 936−940.
(36) Yang, M. J.; She, Y.; Li, Y. Humidity Sensitive Properties of Quaternized Poly (4-Vinylpyridine-Co-Butyl Methacrylate). *J. Mater. Sci. Lett.* **2002**, *21*, 1477−1479.
(37) Xu, R.; Wang, D.; Zhang, J.; Li, Y. Shape-dependent Catalytic Activity of Silver Nanoparticles for the Oxidation of Styrene. *Chem. - Asian J.* **2006**, *1*, 888−893.
(38) Ai, L.; Jiang, J. Catalytic Reduction of 4-Nitrophenol by Silver Nanoparticles Stabilized on Environmentally Benign Macroscopic Biopolymer Hydrogel. *Bioresour. Technol.* **2013**, *132*, 374−377.